# Device modeling of long-channel nanotube electro-optical emitter

J. Tersoff*, Marcus Freitag, James C. Tsang, and Phaedon Avouris
*IBM Research Division, T. J. Watson Research Center, Yorktown Heights, New York 10598*
(Dated: February 2, 2008)

We present a simple analytic model of long single-wall nanotube electro-optical emitters, along with experimental measurements using improved devices with reduced hysteresis. The model describes well the voltage-controlled motion of the emission spot, and provides a clear picture of the physical mechanism of device operation. It also indicates that the electric field is strongly enhanced at the emission spot, and that device performance can be greatly improved by the use of thinner gate oxides.

Carbon nanotube field-effect transistors (CNFETs) exhibit unique electro-optical properties. In particular, they can serve as electrically pumped nanoscale light emitters [1]. Not only is the light source localized to the width of tube (∼1-2nm); it is also localized along the length of the tube, and can be *electronically positioned* [2]. This suggests novel possibilities for electro-optical devices. In addition, such devices provide a unique probe of the transport in nanotubes, because the movable emission spot provides a direct measure of the charge rearrangement in response to voltage changes.

Here we examine the device properties, both theoretically and experimentally, to provide a clear and simple picture of the device behavior. The experiment uses PMMA-passivated devices to reduce the hysteresis seen in past work, allowing better comparison with calculated characteristics. The calculations use a simple quasi-classical model to describe the diffusive transport of electrons and holes along a long semiconducting nanotube. This approach highlights the novel but simple physics underlying the device operation.

We predict a "universal" behavior, with *no adjustable parameters* other than the overall voltage and current scale. This prediction is directly compared with experimental data for the motion of the light-emitting spot, and for the electrical characteristics. The agreement in Figure 1 is striking, in light of the simplicity of the model, and the residual hysteresis in the experimental data.

This gives us confidence to apply the model, to extract information about the transport, the field distribution, and the performance improvements available by oxide scaling. We find that there is a strong enhancement of the electric field near the emission spot, consistent with experimental observations [2, 3]. The device performance is predicted to improve dramatically with reduced gate-oxide thickness, due to both improved gate-channel capacitance and reduced voltage drop at the contacts.

Single-wall carbon nanotubes are grown by chemical vapor deposition [2, 4] on degenerately doped silicon with 100nm silicon oxide. CNFETs are fabricated as described in [2]. The channel length is ∼60 $\mu$m. We observe a strong hysteresis in the as-fabricated devices [2] that can be attributed to the trapping and de-trapping of charges in the gate insulator and/or at states at the $SiO_2$ surface

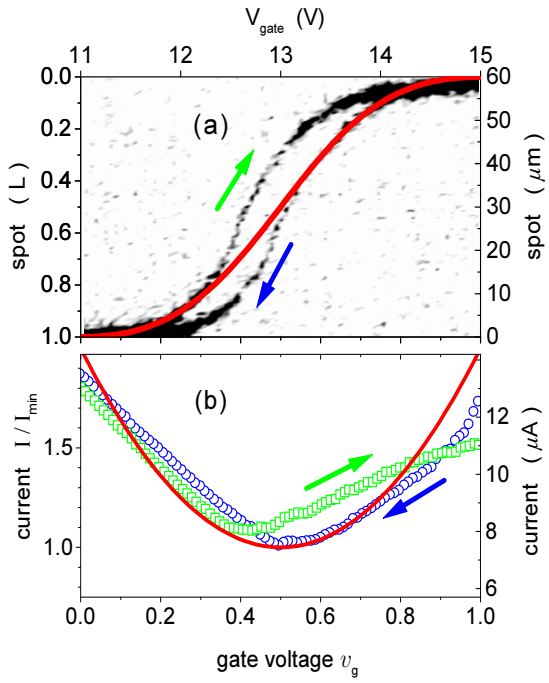


FIG. 1: Measured and calculated characteristics of electroluminescent CNFET. (a) Position of light-emission spot (from drain electrode), and (b) drain current $I$, vs gate voltage $V_g$. Experiment is for $V_d = 15V$. Top and right scales show absolute units for experimental data. Left and bottom scales show scaled units for comparison with theory. Solid red curves are theory, Eqs. (7-8). Experimental data is shown as raw image in (a); a video is also available [10]. Data for current in (b) are shown as open circle and squares. Some hysteresis is visible between forward and reverse $V_g$ sweeps in (a) and (b); direction of each sweep is indicated by an arrow. (There is also an unknown overall shift of the gate voltage scale due to charge trapped in the oxide.)

close to the carbon nanotube. To reduce this effect, we cover the device with PMMA and bake it out on a hot plate in air for 24h at 170C [5]. This procedure greatly reduces the hysteresis observed in the as-fabricated devices. There is apparently still some charge in the oxide, but its effect can be approximated as an overall shift of the $V_g$ scale. We measure the localized infrared emission at $\lambda$=2.0 $\mu$m during gate-voltage sweeps with a liquid

nitrogen-cooled HgCdTe detector array, mounted on top of the camera port of an optical microscope with 50x NIR objective lens [2].

We develop an explicit analytic description of the device properties, based on the physical picture outlined in Ref. [2]. Detailed simulations by Guo and Alam [6] support this qualitative picture. To model diffusive transport along semiconducting nanotubes, we take the current to be

$$I = -m\eta\left(x\right)\frac{dV\left(x\right)}{dx} \tag{1}$$

where $x$ is the direction along the tube (from drain to source), $m$ is the carrier mobility, $\eta$ is the linear density of carriers, and $V$ is the electrostatic potential. Charge conservation in the steady state requires that $I$ is the same for all $x$, so $\eta$ and $V$ cannot vary independently.

Because the gate oxide thickness is much less than the channel length, the nanotube is very effectively screened by the gate. Therefore the potential on the tube is determined by the gate voltage and the local charge [2], and can be approximated as

$$V\left(x\right) = V_g + C^{-1}\rho\left(x\right) \tag{2}$$

where $V_g$ is the gate voltage, $C$ is the nanotube capacitance per length, and $\rho$ is the linear charge density.

Several aspects of the real system are simplified or neglected here. In particular, we use the classical capacitance, neglecting the variation in chemical potential with charge density. And we treat the potential as a strictly local function of charge density, which is only valid on length scales larger than the gate-oxide thickness. We also neglect the dependence of mobility on electric field and charge density. It is possible to avoid some of these simplifications in numerical simulations [6]; and though performed in a relatively short-channel regime, those simulations give confidence in the appropriateness of our simplified treatment.

In keeping with our focus on long length scales, we also assume a negligible recombination length, so at any $x$ there can be electrons or holes but not both. Then $\rho = \pm\eta$ (positive for hole region), and combining Eqs. (1) and (2) gives

$$\frac{dV\left(x\right)}{dx} = \mp\frac{I}{mC\left[V\left(x\right) - V_g\right]} \tag{3}$$

This equation can be solved analytically in each region. The boundary conditions on $V\left(x\right)$ are $V_{s1}$ and $V_{d1}$ (the potential on the nanotube at the source and drain ends), and $V = V_g$ at the point separating electron and hole regions. We focus on the ambipolar regime where light emission is possible, which for $I > 0$ is $V_{d1} \geq V_g \geq V_{s1}$. Then

$$V\left(x\right) = V_g \pm \left(\frac{2I}{mC}\right)^{1/2}\left|x - x_0\right|^{1/2} \tag{4}$$

where $\pm$ is $-1$ for electrons and $+1$ for holes. Also

$$x_0 - x_d = L\left[\frac{\left(V_{d1} - V_g\right)^2}{\left(V_{s1} - V_g\right)^2 + \left(V_{d1} - V_g\right)^2}\right] \tag{5}$$

where $x_0$ is the point separating electron and hole regions, and $L = x_s - x_d$ is the channel length, $x_s$ and $x_d$ being the positions of the source and drain contacts, respectively. Combining these gives

$$I = \frac{mC}{2L}\left[\left(V_{s1} - V_g\right)^2 + \left(V_{d1} - V_g\right)^2\right] \tag{6}$$

in the ambipolar regime.

The equations above refer only to diffusive transport along the channel, and do not include contact effects. Electrical contacts to nanotubes are a rich subject in their own right — the transmission depends on both the Schottky barrier height and the electrode geometries [7, 8], and no doubt also on other factors that are less well understood. In general there is a voltage drop $V_c$ associated with each contact, in addition to the continuous voltage drop along the tube. For the ambipolar case there is necessarily a voltage drop, equal to the bandgap, associated with the crossover from electron to hole conduction, which in our model means that $V_c$ cannot be less than the Schottky barrier height. Because of the highly nonlinear behavior of Schottky contacts, we treat $V_c$ as constant here (and assumed to be the same for both contacts) in the ambipolar regime, analogous to a threshold voltage [9].

Then following the usual convention that $V_s = 0$ and $V_d$ denotes the applied drain voltage, we have $V_{s1} = V_c$ and $V_{d1} = V_d - V_c$ in the ambipolar regime. Combining this with Eqs. (5-6), we can describe the behavior in a scale-free way, as

$$\frac{I}{I_{\min}} = 2\left[v_g^2 + \left(1 - v_g\right)^2\right] \tag{7}$$

$$\frac{x_0 - x_d}{L} = \frac{\left(1 - v_g\right)^2}{v_g^2 + \left(1 - v_g\right)^2} \tag{8}$$

Here $V_d - 2V_c$ is the range of gate voltage over which the emission spot sweeps from source to drain; $v_g = \left(V_g - V_c\right)/\left(V_d - 2V_c\right)$ is the gate voltage as a fraction of this total sweep voltage; and $I_{\min} = \left(mC/4L\right)\left(V_d - 2V_c\right)^2$ is the minimum current, which occurs at $v_g = 1/2$.

Our device measurements and model calculations are summarized in Figure 1. (A movie of the experimental spot motion is also available [10].) Figure 1b shows the gate voltage characteristic of the device and Figure 1a shows the corresponding movement of the light-emission spot along the carbon nanotube. The experimental measurements can be put directly on the same dimensionless scale as the model, by noting that $v_g = 0$ and 1 are the gate voltages at which the spot reaches the source and

drain. The overall agreement between the measured characteristics and model calculations in Figure 1 is striking. The spot moves rapidly with $V_g$ when in the middle of the channel, and more slowly near the source and drain. The shape of the spot-motion curve is very well reproduced. The current variation is also rather well reproduced, to the extent of capturing the symmetric minimum and general magnitude of variation. The remaining discrepancies are attributable in part to the residual hysteresis seen in the experiment. However, the approximations of constant mobility and constant voltage drop at the contacts also play a role, we expect.

The experimental data also provide a direct determination of $V_c$. In Fig. 1a, $V_d = 15$V, while the spot sweeps from source to drain over a $V_g$ range of $\approx 4$V. Equating this range with $V_d - 2V_c$ suggests that $V_c \sim 5 - 6$V. This is consistent with typical threshold voltages observed for nanotube Schottky-barriers transistors on such thick gate oxides.

Combining Eqs. (2), (4), and (6), and incorporating $V_c$, gives the charge density,

$$\rho\left(x\right) = \pm\rho_d \left[\left(v_g\right)^2 + \left(1 - v_g\right)^2\right]^{1/2} \left|\frac{x - x_0}{L}\right|^{1/2} \qquad (9)$$

where $\rho_d = C\left(V_d - 2V_c\right)$. Figure 2 shows the calculated charge and electrostatic potential along the tube for different values of the gate voltage. Within our model, the carrier density goes to zero at the ambipolar emission spot, while the electric field driving the current diverges there, as

$$\frac{dV}{dx} = -\left(\frac{I}{2mC}\right)^{1/2} \left|x - x_0\right|^{-1/2} \qquad (10)$$

Of course, in reality there is some overlap of electron and hole regions due to the finite recombination rate; so this singularity is smoothed into a peak. Still, the enhancement of electric field in the recombination region has important consequences. It leads to strong hot-carrier effects in electroluminescence [3], and increases the likelihood of Zener tunneling at defects [2].

Our results suggest that such electroluminescence devices can be dramatically improved by using thinner oxides, and further improved by using high-k dielectrics. A major limiting factor is the high voltage required. But most of the voltage drop apparently occurs at the contact. The threshold voltage for the contacts scales with oxide thickness, and can be further improved by optimizing the contact geometry and using different gate dielectrics [7, 8]. Thus it should be possible to reduce the voltage drop $V_c$ by an order of magnitude. The voltage drop along the channel scales as $C^{-1}$, so this can also be greatly reduced with a thin high-k gate dielectric. In this way the device could operate at lower voltages and higher currents, give brighter and more efficient light emission.

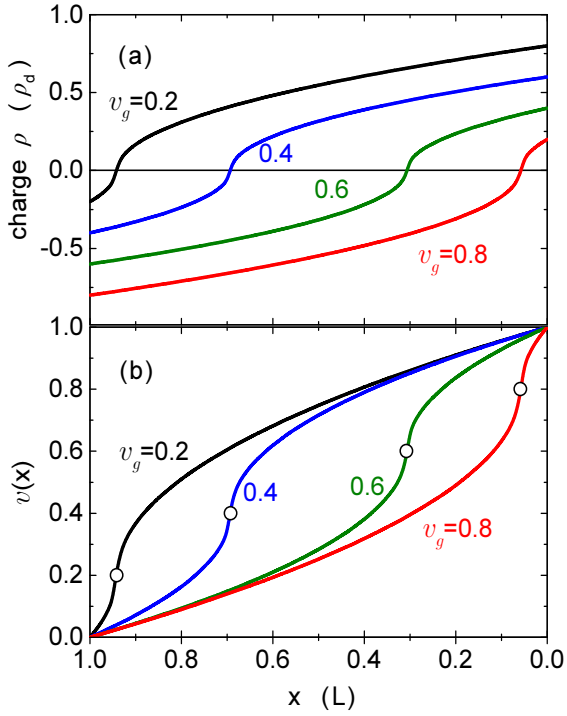


FIG. 2: (a) Charge density [Eq. (9)], and (b) electrostatic potential [Eq. (4)], along the nanotube (as fraction of channel length $L$, with drain at right), for fixed drain voltage $V_d$ and different values of scaled gate voltage $v_g$. Here $v(x) = (V(x) - V_c)/(V_d - 2V_c)$. Curves from left to right correspond to $v_g = 0.2$, 0.4, 0.6, and 0.8. Circles indicate where $v = v_g$ and $\rho = 0$.

We acknowledge Q. Fu and J. Liu for providing us with long CVD-grown carbon nanotubes, J. Chen for helpful discussions, and B. Ek for expert technical assistance.

[*] Electronic address: tersoff@us.ibm.com

[1] J. A. Misewich, R. Martel, Ph. Avouris, J. C. Tsang, S. Heinze, and J. Tersoff, Science 300, 783 (2003).
[2] M. Freitag, J. Chen, J. Tersoff, J. C. Tsang, Q. Fu, J. Liu, and Ph. Avouris, Phys. Rev. Lett. 93, 076803 (2004).
[3] M. Freitag, V. Perebeinos, J. Chen, A. Stein, J. C. Tsang, J. A. Misewich, R. Martel, and Ph. Avouris, Nano Lett. 4, 1063 (2004).
[4] S. Huang, X. Cai, and J. Liu, J. Am. Chem. Soc. 125, 5636 (2003).
[5] W. Kim, A. Javey, O. Vermesh, Q. Wang, Y. Li, H. Dai, Nano Lett. 3, 193 (2003).
[6] J. Guo and M. A. Alam, Appl. Phys. Lett. 86, 023105 (2005).
[7] S. Heinze, J. Tersoff, R. Martel, V. Derycke, J. Appenzeller, and Ph. Avouris, Phys. Rev. Lett. 89, 106801 (2002).
[8] S. Heinze, M. Radosavljević, J. Tersoff, and Ph. Avouris, Phys. Rev. B 68, 235418 (2003).
[9] M. Radosavljević, S. Heinze, J. Tersoff, and Ph. Avouris, Appl. Phys. Lett. 83, 2435 (2003).

[10] See EPAPS Document No. ___ for a movie of the moving emission spot. This document may be retrieved via the EPAPS homepage (http://www.aip.org/pubservs/epaps.html) or from ftp.aip.org in the directory /epaps/. See the EPAPS homepage for more information.